Spectrochimica Acta Part B 64 (2009) 999–1008

Contents lists available at ScienceDirect

Spectrochimica Acta Part B

journal homepage: www.elsevier.com/locate/sab

Semiempirical model for analysis of inhomogeneous optically thick laser-induced plasmas ☆

Cristian A. D'Angelo [a,b], Diego M. Díaz Pace [a,c,*], Graciela Bertuccelli [a,c]

[a] Instituto de Física 'Arroyo Seco,' Facultad de Ciencias Exactas, U.N.C.P.B.A., Campus Universitario, Paraje Arroyo Seco, (B7000GHG) Tandil, Buenos Aires, Argentina
[b] CICPBA, calle 526 entre 10 y 11, 1900 La Plata, Argentina
[c] CONICET, Rivadavia 1917, 1033 Buenos Aires, Argentina

ARTICLE INFO

Article history:
Received 28 November 2008
Accepted 6 July 2009
Available online 16 July 2009

Keywords:
LIBS
Optically thick plasma
Inhomogeneous plasma
Metallic alloys

ABSTRACT

In this paper, a more realistic approach of a non-uniform optically thick plasma in local thermodynamic equilibrium was applied to describe self-reversal of Co I 340.51 nm emission line recorded from a laser-induced plasma generated on a Co–Cr–Mo metallic alloy. This line was selected because it is one of the most absorbed of the major elements in air at atmospheric pressure.

The model describes the behavior of the plasma after the breakdown, and it was semiempirical thus, some information was taken from the experiment. A cylinder-symmetrical plasma column with a parabolic temperature distribution having a maximum at the center and decreasing toward the edges was considered. The input parameters were the plasma length, the temperature in the plasma core, and the Co total density, which were estimated from measurements and previous work. Moreover, the distribution of electron density depended on the temperature, and the ionization degree was taken into account through Saha equation. Then, plasma parameters were adjusted in such a way calculations reproduced the experimentally measured line profiles.

The effect of varying laser power on plasma homogeneity and its evolution in time were investigated. Moreover, preliminary results of spatial distribution of plasma parameters were obtained that confirmed the practical application of the model on plasma diagnostics.

1. Introduction

Laser-induced breakdown spectroscopy (LIBS) is a technique based on the spectral analysis of the radiation emitted by a plasma produced by focusing a laser pulse on the target surface. In typical LIBS conditions, laser-induced plasmas (LIPs) can be characterized by analyzing the emitted spectral lines through the determination of their main parameters such as the temperature, the electron density, and the atom/ion densities of the different species present in the plasma plume. This is an issue of prime importance in order to both improve the applications and get a deep insight of its fundamentals to establish LIBS as an analytical method, which is very promising in several areas as plasma physics, industry, environment (i.e.: air, water, soil), cultural heritage, remote analysis in hostile environments, and for safety and security [1].

The most widely used methods to characterize a LIP involve a Boltzmann Plot to calculate the plasma temperature, measurement of Stark line-broadening to estimate the electron density, and calibration curves constructed with reference samples to obtain the elemental composition [2]. Many papers have been devoted to plasma characterization in several kinds of samples under different experimental conditions [3–10]. Nevertheless, some concerns may arise in some specific situations.

First, those procedures require that the measured spectral lines are emitted in optically thin conditions. Actually, in LIPs generated at atmospheric pressure, which are experimentally simpler and are usually used in several applications, self-absorption of the spectral lines occurs due to the high density of atoms and ions present within the plasma, which is said optically thick. As a consequence, the intensity of the lines saturate depending on its spectroscopic features and the experiment [11–14]. Second, it is well known that LIPs are inhomogeneous sources because of the existence of temperature gradients inside the plasma plume. Thus, the emission intensity along the line of sight includes contributions from plasma regions with different values of the plasma parameters. In an inhomogeneous optically thick LIP strongly absorbed lines result self-reversed [15,16].

☆ This paper was presented at the 5th International Conference on Laser-Induced Breakdown Spectroscopy (LIBS 2008), held in Berlin, Adlershof, Germany, 22-26 September 2008, and is published in the Special Issue of Spectrochimica Acta Part B, dedicated to that conference.

* Corresponding author. Pinto 399, B7000GHG Tandil, Buenos Aires, Argentina. Tel.: +54 2293 439660/1; fax: +54 2293 439669.
E-mail addresses: cdangelo@exa.unicen.edu.ar (C.A. D'Angelo), ddiaz@exa.unicen.edu.ar (D.M. Díaz Pace), gbertucc@exa.unicen.edu.ar (G. Bertuccelli).

0584-8547/$ – see front matter © 2009 Elsevier B.V. All rights reserved.
doi:10.1016/j.sab.2009.07.006

Moreover, reference samples are not available when dealing with unique, unknown, complex or expensive samples. Thus, either calibration curves cannot be constructed or are affected by strong matrix effects [17–22].

To overcome those drawbacks, several works have been dedicated to the research of an alternative LIBS analysis based on plasma physics to characterize the plasma state, under the assumptions that (i) the plasma composition is representative of that of the target (stoichiometric ablation), and (ii) the plasma is in local thermal equilibrium (LTE) [23–26]. In an optically thin inhomogeneous plasma with cylindrical symmetry, the characterization of the plasma with spatial resolution can be achieved from a deconvolution procedure of the emissivity, such as the Abel inversion [27–29]. Furthermore, other papers have been reported about modeling the postbreakdown LIP expanding into an ambient gas. Gornushkin et al. [30] developed a simplified theoretical approach for an optically thick inhomogeneous LIP based on an approach of Bartels and Zwicker [31] that describes the time evolution of one atomic transition and the plasma continuum for a Si/N system in vacuum after the interaction laser-target has ended. This model was further extended to an atmospheric plasma expansion where a shock wave formation was considered [32]. In addition, a two-line method for determination of the maximum temperature in the plasma center along the line of sight assuming a parabolic temperature distribution was successfully applied based in that framework [33]. These works are aimed at spectroscopic applications and provide a simple theoretical framework to match observed spectral features to plasma parameters.

It is well known that self-reversal of spectral lines is originated by inhomogeneities in the plasma, which can be figured out as composed of an internal core and external shells with cold absorbing atoms. Nevertheless, some questions can be risen about this picture. For example, we wonder if the depth of the dip can be used to estimate the plasma inhomogeneity.

In a previous work by our group, a simple model of a two-region plasma was implemented to characterize the physical state of a laser-induced plasma produced on a metallic alloy [34]. The plasma parameters that reproduced the experimental profiles were obtained by a fitting procedure carried out by a self-made computer program which took into account self-absorption as well as plasma inhomogeneity, and without employing any reference sample. This was a first step to investigate plasma characterization through the profiles of previously selected spectral lines, which is very useful in terms of understanding processes taking place inside the plasma and its dependence upon the experimental conditions. In this work, the two-region plasma model is improved to a more real non-uniform plasma with a temperature distribution inside the plasma plume (e.g., parabolic) which is intended to both validate the model with the experiment and understand how the plasma parameters affect the features of the emission profiles.

The model was applied for LIPs diagnostic from the shape of one measured spectral line, which was selected as the most suitable for plasma characterization in our experiment. In this approach, the effects of varying laser energy and evolution in time on plasma homogeneity were investigated. In fact, The laser pulse energy is a critical parameter in LIBS analysis since, for a given focusing distance, it determines the laser irradiance onto the target, which manages the process of plasma formation by absorption of the laser radiation [35]. In addition, some preliminary results of the applicability of the model on spatially-resolved plasma diagnostics are presented.

2. Theoretical: inhomogeneous optically thick plasma in LTE

We consider a cylinder-symmetrical optically thick inhomogeneous plasma column in local thermal equilibrium (LTE) with an emission coefficient ε_ν (J s^{-1} m^{-3} sr^{-1} Hz^{-1}) and an absorption coefficient $\kappa(\nu)$ (m^{-1}) distributed within the plasma volume. The intensity I_ν (J s^{-1} m^{-2} sr^{-1} Hz^{-1}) emitted along the line of sight (x coordinate) is given by the equation of radiation transfer (Fig. 1) [31],

$$I_\nu = \int_{-x_0}^{x_0} \varepsilon_\nu(x) \exp\left[-\tau(\nu,x)\right] dx, \tag{1}$$

where $\tau(\nu,x)$ (dimensionless) is the optical thickness of the plasma at position x, given by

$$\tau(\nu,x) = \int_{x}^{x_0} \kappa(\nu,x)dx. \tag{2}$$

The total optical thickness along the line of sight is

$$\tau_0(\nu) = \int_{-x_0}^{x_0} \kappa(\nu,x)dx, \tag{3}$$

where x_0 and $-x_0$ refer to the plasma size along the direction of observation.

For an homogeneous plasma with absorption and emission coefficients $\kappa(\nu)$ and $\varepsilon(\nu)$ Eqs. (1) and (3) become

$$I_\nu = S_\nu\left(1 - e^{-\tau(\nu)}\right), \tag{4}$$

$$\tau_0 = \kappa(\nu)\, l, \tag{5}$$

with $S_\nu = \varepsilon_\nu/\kappa_\nu$ the source function and l the length of the emitting plasma.

For an inhomogeneous plasma, it has been shown that in the absence of stimulated transitions, Eq. (1) can be written as [31]

$$I_\nu = C\, S_\nu(T_m).M.Y(\tau_0,p), \tag{6}$$

where S_ν is the source function that depends on the maximum plasma temperature (T_m) and C a factor that unifies units and depends on the experimental conditions. M is a factor that takes into account the degree of inhomogeneity of the column. It is a factor by which the emission along the line of sight of the inhomogeneous plasma is smaller then the emission of a homogeneous plasma with the same optical thickness τ_0. $M = 1$ in the limit of an homogeneous layer, and

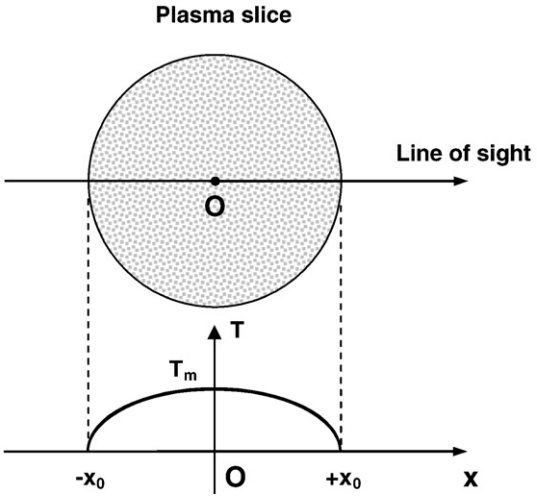

Fig. 1. Observation geometry and plasma temperature profile.

smaller than unity for more inhomogeneous plasmas. For Stark broadened neutral lines,

$$M = \frac{E_i + 0.5\chi_0}{E_j + 0.5\chi_0} \quad \text{if} \quad \frac{kT_m}{E_i + 0.5\chi_0} \ll 1. \tag{7}$$

with c_0 the ionization energy. $Y(\tau_0,p)$ is a function that represents the influence of the optical thickness τ_0 on the measured intensity, and that can be approximated starting from a parameter p. It is well approximated by

$$Y[\tau(\nu,x),p] = e^{\frac{-\tau(\nu,x)}{2}}\left[\frac{-\tau(\nu,x)}{2}(1-p) + p\sinh\left(\frac{-\tau(\nu,x)}{2}\right) + \frac{1}{\sqrt{p}}\sinh\left(\frac{-\tau(\nu,x)}{2}\sqrt{p}\right)\right], \tag{8}$$

where

$$p = \frac{6}{\pi}\left(\frac{M^2}{\sqrt{1+M^2}}\right). \tag{9}$$

Neglecting induced transitions, the maximum value of the source function is given by

$$S_{\nu max} = \frac{2h\nu^3}{c^2}\exp\left(-\frac{h\nu}{kT_m}\right), \tag{10}$$

Substituting the values calculated by Eqs. (7)–(10) into Eq. (6) allows computing the spectral emission intensity, I_ν, for an optically thick non-homogeneous plasma.

3. Experimental

The experimental setup consisted of a good spectral resolution system based on a photomultiplier tube (Fig. 2). It was already described in a previous work, so it will be briefly outlined here. The plasma was generated by focusing a Nd:YAG laser (λ = 1064 nm, 7 ns pulse FWHM) running at a 2 Hz repetition rate onto the sample surface in air at atmospheric pressure. The target was a metallic Co–Cr–Mo alloy with nominal concentrations of 63% Co, 30% Cr and 7% Mo fixed to a rotary holder. The pulse energy was set in the range 35–75 mJ. The plasma plume was imaged on the entrance slit (40 μ-width) of a spectrograph (Czerny-Turner, resolution 0.01 nm, focal length 0.5 m, grating of 2400 lines/mm) by means of a second lens. The detector was a photomultiplier (PM) whose signal was time resolved and averaged with a Box-Car.

The emission line profiles were scanned by moving the diffraction grating of the monochromator, which was controlled by software and synchronized with the data acquisition and the laser firing. In order to get spatially-resolved measurements of the plasma, a quartz lens was mounted on a translation stage allowing the collection of light from different slices of the plasma perpendicular to the direction of plume expansion. Then, by moving the image formed on the entrance slit of the monochromator, the emission of the plasma from its brightest region (core) was selected. For the present experiment, the emission from the plasma core, spatially integrated along the line of sight, was recorded around the strong Co I 340.51 nm line ($A_{ji} = 1\times10^8$ s^{-1}, $E_i =$ 0.43 eV, $E_j = 4.07$ eV, $g_i = 10$, $g_j = 10$, $c_0 = 7.88$ eV) with delay times between 4 and 12 ms after the laser pulse, where each experimental point was obtained averaging three laser shots. The laser irradiance at the sample surface was varied by changing the pulse energy in the range of 35–75 mJ, which was measured with a calorimeter, by means of an optical attenuator, maintaining the lens-to-sample distance in such a way that it was lower than the focal length.

4. Results and discussion

4.1. The model

In the framework of a collision-dominated plasma in LTE, the line intensity profile of a strong non-resonant atomic transition is calculated using Eq. (6), as well as standard statistical distributions. The input parameters are the initial plasma length, the temperature in the plasma core, and the total density of Co, which were estimated in a previous work from the simpler 2-region approach [34]. The model is semiempirical so some information is obtained from the experiment (i.e.: the temperature gradient) matching the computed profiles to the measurements. The model outputs are spatial distributions of species

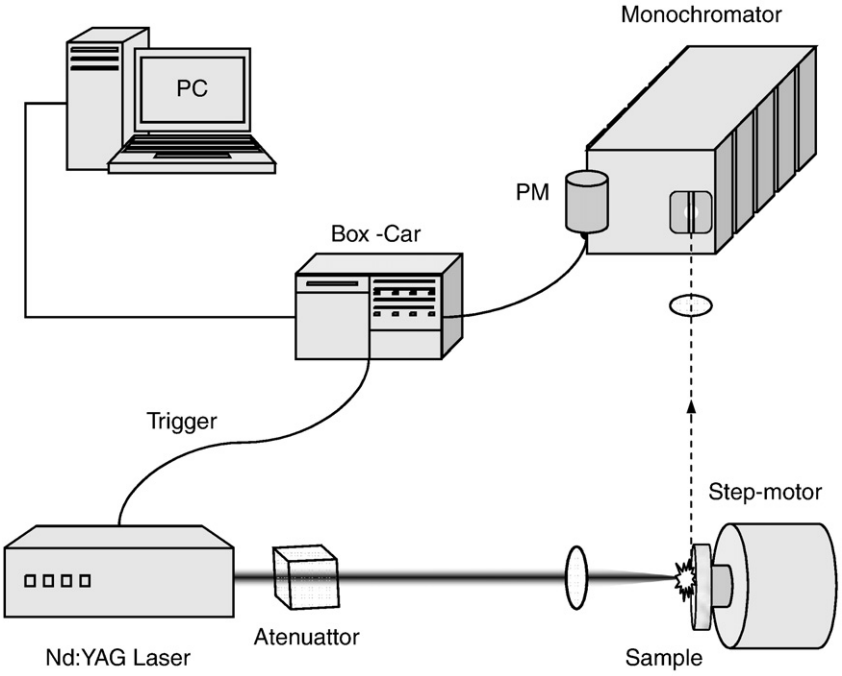

Fig. 2. Experimental setup.

in the plasma plume (atoms, ions and electrons). The following assumptions are made on the specific properties of the plasma:

(i) A cylinder-symmetrical plasma expanding into air with an estimated initial diameter of ~2 mm, depending on laser energy, and decreasing as the plasma cools down, is considered.
(ii) In atmospheric conditions, the leading edge of the expanding plasma interacts with the surrounding air originating a shock wave. In spite of this, the boundary effects are ignored to make the model simpler.
(iii) The temperature distribution is simulated by a second-order polynomial with its maximum in the plasma center (T_m) and declining toward plasma edges,

$$T(x) = T_m\left(1 - bx^2\right), \tag{11}$$

where x is the coordinate along the direction of observation, and b (m^{-2}) is a coefficient related to the spatial temperature gradient, which is going to be determined from the experiment.
(iv) It is assumed that the dynamics of the electron density follows the same trend that the temperature. This has been demonstrated in the work of ref. [27], where the spatial distribution of the electron density reaches its maximum value at the plasma center and decreases smoothly for increasing radial distances. Hence, a dependence of the electron density upon the plasma temperature expressed by a second-order parabola is used.
(v) Since the dominating line-broadening mechanism in LIPs is Stark broadening, the line profile is expressed by the Lorentzian function with a line-width (FWHM) given by [36]

$$w = C\ \langle n_e\rangle\ \langle T\rangle^{1/6}, \tag{12}$$

where the value of the C constant was estimated from [37], and a spatial averaging over the plasma length of both temperature and electron density are employed.
(vi) The total Co density is supposed uniformly distributed throughout the plasma. This does not mean that the spatial distribution of species in different ionization stages are uniform. Actually, since LTE holds, we can calculate atom and ion densities distributions using Saha and Boltzmann equations. Moreover, we consider the approximation that the total density of Co species in the plasma is $N_{Co} = N_{CoI} + N_{CoII}$, as discussed in Section 4.3.

4.2. Analysis of the emission profiles

According to Eq. (6) the line intensity is related to the temperature in the plasma center through the source function. In fact, a higher value of T_m implies a raise of the emission line intensity. Moreover, as explained in [31], since M and p are approximately constant within the line, and the source function is independent of the wavelength with good approximation, the wavelength distribution of the emitted intensity is determined only by the function $Y(\tau_0,p)$. When the optical thickness in the line centre (τ_0) reaches a critical value ($\tau_{0c}\approx 2$), corresponding to the maximum of the Y-curve, the line is top-flattened and the intensity has the maximum value possible. Further enlargement of the optical thickness exceeding the critical value ($\tau_0 > \tau_{0c}$) originate self-reversal with such a depth of the central dip tied to the value of τ_0.

In Fig. 3 the dependence of τ_0 upon the parameters of the model (the temperature in the plasma core T_m, the diameter d, and the gradient of temperature b), is analyzed. The total particle density was 10^{16} cm^{-3}. While each curve in Fig. 3a represents the calculated values of τ_0 corresponding to plasmas with the same T_m and diameter, but with different degree of homogeneity, in Fig. 3b the values of τ_0 for different T_m and fixed gradient and length values are shown. Fig. 3c,d depicts the parabolic profiles of temperature along the line of sight in each case. Fig. 3e,f shows plots of the computed lateral distribution of the population density of the lower level of the transition (n_i). In Fig. 3g,h the computed line profiles in each case are shown. It can be seen that the variation of plasma homogeneity makes τ_0 to reach a maximum for a certain value of b. The maximum of τ_0 decreases and moves toward a higher gradient as T_m grows (Fig. 3a). This can be explained from Fig. 3c,e: as temperature gradient increases, the plasma edges cold down so, first there is an absorption raise in that region as a result of an increasing population of the lower level of the transition. After that, absorption drops because the population of that level declines. Hence, the maximum of τ_0 is related to the maximum of population of the lower level of the involved transition. In this case, the intensity of the two maxima relative to the depth of the central dip is the same for all the profiles (Fig. 3g). On the other hand, τ_0 decreases monotically as a consequence of a drop of temperature where the spatial distribution remains the same (b = const), and T_m falls down (Fig. 3b,d), as well as do the lower level population in the plasma boundaries (Fig. 3f). In this situation, the depth of the central dip decreases accordingly to the values of τ_0.

From this previous analysis, it can be realized that the optical thickness is the key since it saves all the information about the line. Thereby, a qualitative interpretation of the behavior of the plasma parameters starting from line features can be achieved, and quantitative results can be obtained matching the computed profiles to the experiment. This is carried out in Section 4.4.

4.3. Lines and measurements

In a previous work, we employed a simpler approach of a two-region plasma to achieve analytical results from the experimental profiles of selected spectral lines of the major elements of the target (i.e.: Co and Cr). It allowed us to obtain an estimation of the values of the plasma parameters that are here revised and used for either preliminary analysis or as initial input parameters.

For a plasma in LTE, the total optical depth of Eq. (5) can be expressed as [13]

$$\tau_0 = \kappa(\lambda)\, l = \kappa_e\, N\, l\, g(\lambda). \tag{13}$$

In this expression, κ_e (m^3) is a factor that depends on the atomic parameters of the transition and can be calculated if the plasma temperature is known. Namely

$$\kappa_e = \frac{\lambda^4}{8\pi c Q} A_{ji} g_j e^{-E_i/kT}\left(1 - e^{\frac{E_i - E_j}{kT}}\right), \tag{14}$$

where N (m^{-3}) is the density of the emitters in the plasma, l (m) is the absorption path-length and $g(\lambda)$ (m^{-1}) is the normalized line shape. Moreover, Q (dimensionless) is the atomic partition function, A_{ji} (s^{-1}) is the transition probability, g_j (dimensionless) is the statistical weight and E_i, E_j (eV) are the energy levels. The subscripts i and j refer to the upper and lower levels, respectively.

The κ_e factor of Eq. (14) is useful to predict the expected optical depth for different spectral lines and to know in advance which one will result in a greater or minor absorption in a LIBS experiment. In Fig. 4, the coefficient κ_e is plotted for several Co I transitions as a function of the temperature. We can infer that for the typical range of temperature obtained in our experiment (0.5–1.1 eV) the lines 345.35 nm and 340.51 nm will be the most absorbed in the LIP. As there is a Cr line close to the former, while the later is well isolated and free from interferences from another elements, it was selected as the analytical line. A record of the line is shown in Fig. 5, where it can be

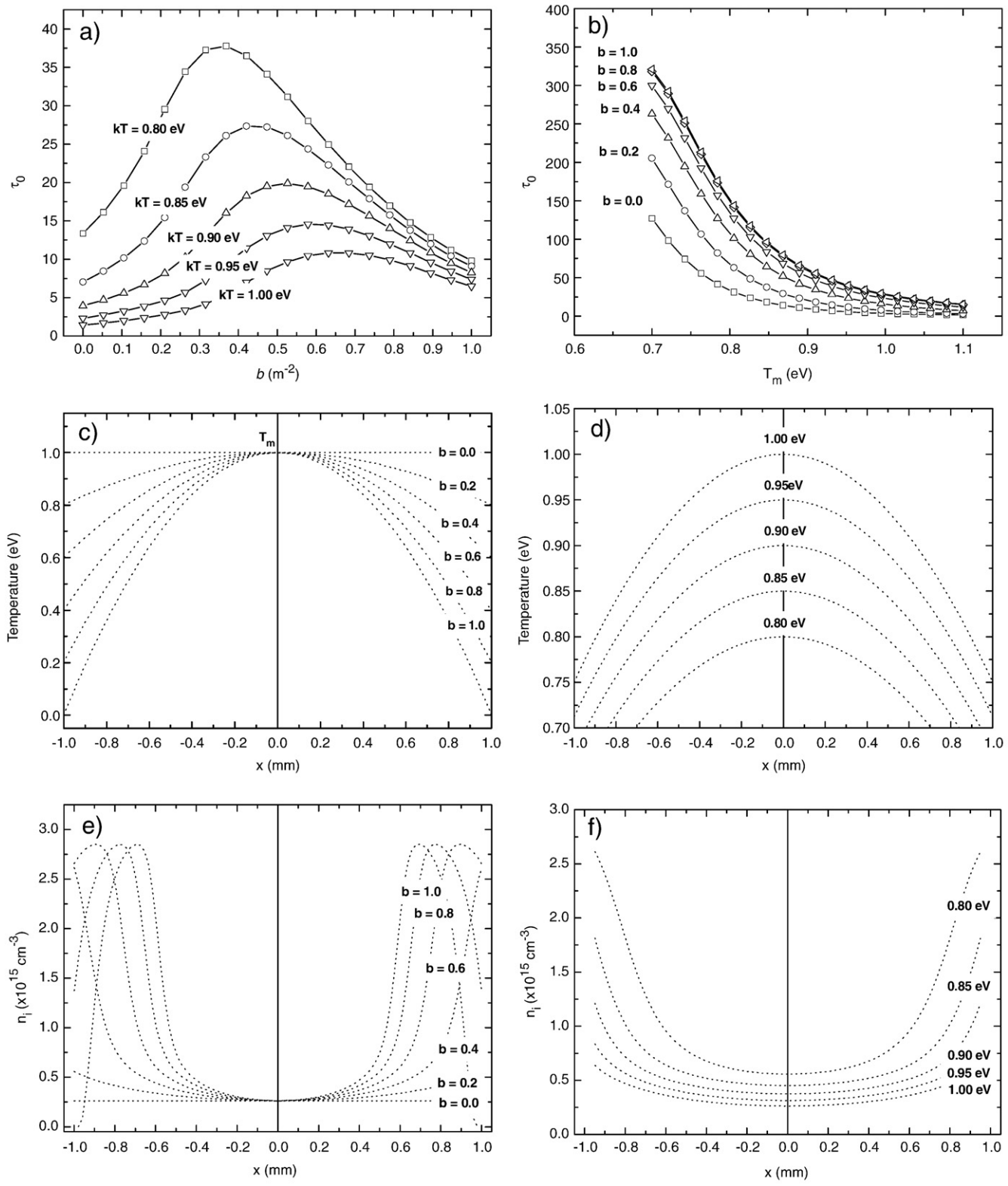

Fig. 3. a) Dependence of the optical thickness t_0 on the gradient of temperature b calculated for fixed values of the temperature in the plasma center T_m and a plasma length of 2 mm. b) Dependence of the optical thickness t_0 on the temperature of the plasma center T_m calculated for fixed values of the temperature gradient b and a plasma length of 2 mm. c) Parabolic profiles of the temperature along the line of sight computed for $T_m = 1$ eV and different gradient values b. d) Parabolic profiles of the temperature along the line of sight computed for a temperature gradient $b = 0.25$ m^{-2} and different temperatures of the plasma center T_m. e) Computed lateral distributions of the population ni (cm^{-3}) of the lower level of the transition 340.51 nm Co I as a function of the temperature gradient b. f) Computed lateral distributions of the population ni (cm^{-3}) of the lower level of the transition 340.51 nm Co I as a function of the temperature of the plasma center T_m. g) Computed profile of the line 340.51 nm Co I for different temperatures of the plasma center T_m , a temperature gradient $b = 0.25$ m^{-2} and a plasma length of 2 mm. h) Computed profile of the line 340.51 nm Co I for different temperatures of the plasma center T_m and temperature gradients b, $t_0 = 0.7$, and a plasma length of 2 mm.

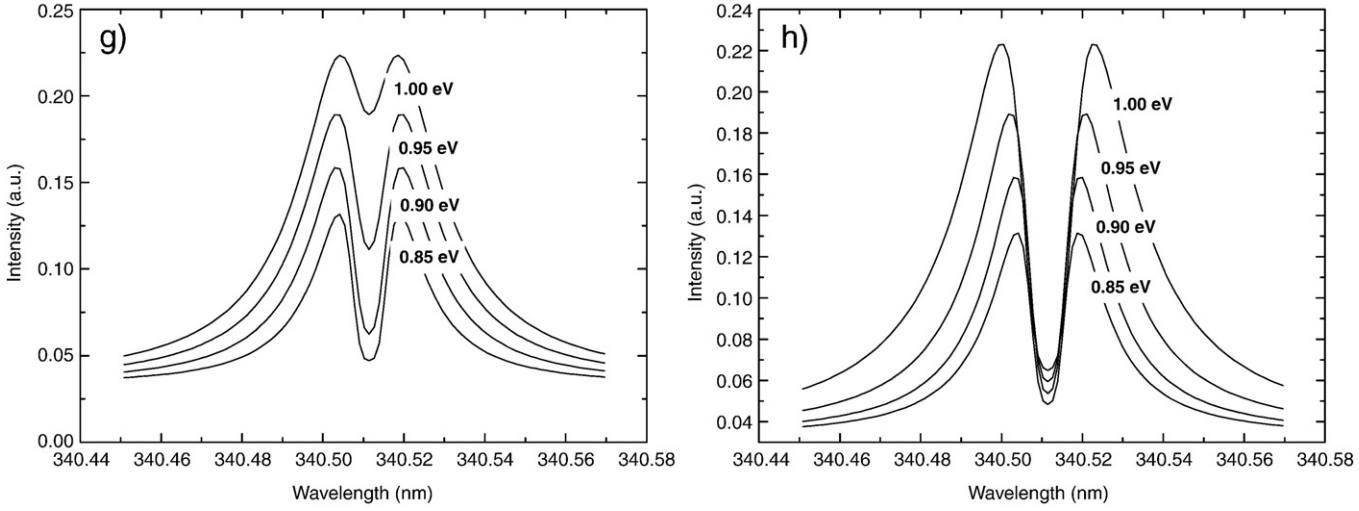

Fig. 3 (*continued*).

seen that this line results strongly self-reversed showing a pronounced dip, a fact that itself reveals that we are dealing with an inhomogeneous thick plasma where a temperature gradient exist.

In addition, ionization stages higher than one do not contribute significantly to the total plasma population. This can be deduced calculating the relative local contributions of the species to the total plasma population using the Saha equation for an electron density of 10^{17} cm^{-3}. As shown in Fig. 6, for plasma temperatures between 0.5 and 1.1 eV the density of the second ion is very small (<0.01%) compared to either atom density or first ion density; therefore, it can be neglected. Moreover, the plasma core is mainly populated by ions, while neutral atoms are preferably situated in the boundaries. Spectroscopic parameters of Co II lines are not available except for few faint lines whose transition probabilities are two orders of magnitude lower than Co I lines, so Co II lines were not measured in this work.

In order to analyze the behavior of plasma parameters under different experimental conditions, the line 340.51 nm was recorded with pulse energies of 35, 45, 55, 65 and 75 mJ, and delay times of 4, 8, 10 and 12 μs.

4.4. Pulse energy and temporal evolution effects

The applicability of the model was evaluated analyzing the influence of laser pulse energy and time evolution. Results exposed in this section were obtained by running the algorithm for estimated initial values of the input parameters, i.e.: $l=2$ mm, $T_m=1$ eV, $N_{Co}=10^{16}$–10^{17} particles/cm^{-3}, and a typical range of values of the temperature gradient, b, i.e.: 0–0.5 m^{-2}. Then, they were varied until a close agreement occurred between the theoretical and the experimentally line profiles of the analytical line Co I 340.51 nm measured with different pulse energies and at different delay times.

As the laser energy was increased, and consequently the irradiance was higher, it was observed a clear growth of the line intensity, and that all the experimental profiles exhibited a central dip with a smaller depth for the higher the irradiance (Fig. 7a). In the frame of our model (see Fig. 3g), we explained the higher emission intensity by a raise of plasma temperature, and a lower value of τ_0 to account for the decrease in the depth of the central dip. Therefore, laser energy effect can be figured out as a downward displacement along a vertical line in Fig. 3a, or as a movement toward the right along one of the curves of Fig. 3b, keeping a constant gradient of temperature in both cases. On the other hand, it was already noticed that for a given pulse energy, the line profile evolved in time decreasing the emitted intensity (as the plasma cools down) but maintaining the ratio between the peak intensity of the two maxima and the depth of the dip (Fig. 7b). Thus, time evolution can be pictured as an horizontal movement in Fig. 3a with a constant value of τ_0 (see Fig. 3h), since it entails the same

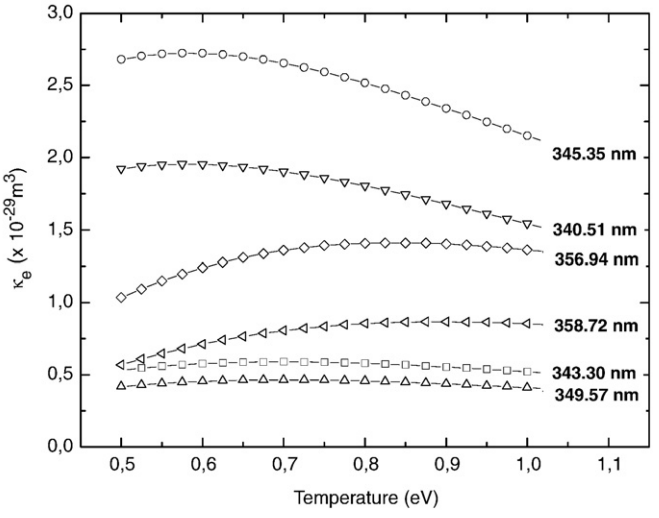

Fig. 4. Factor k_e plotted for the stronger Co I lines as a function of the temperature.

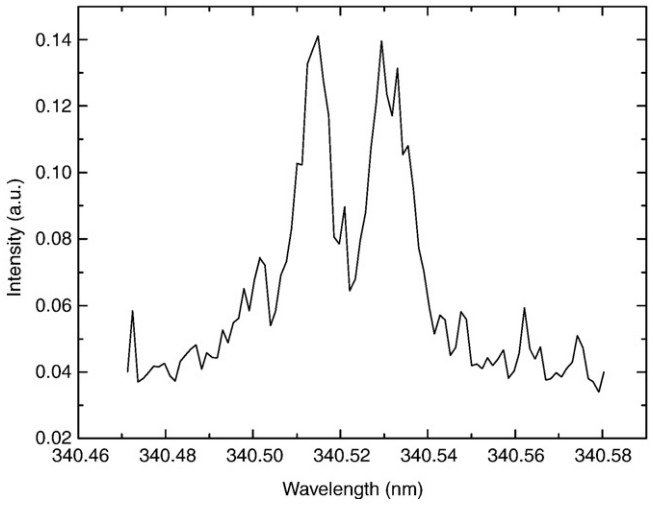

Fig. 5. Line 340.51 Co I showing the characteristic dip of a strongly absorbed and self-reversed line from and inhomogeneous plasma.

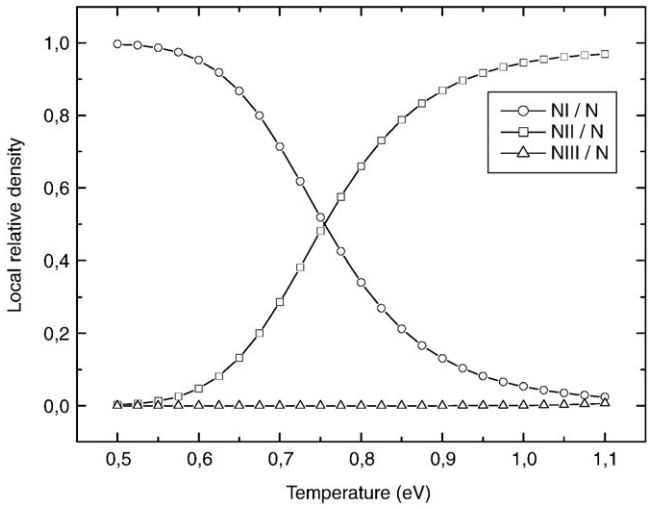

Fig. 6. Relative local populations of Co species calculated for an electron density of 10^{17} cm^{-3}.

relative shape of the line profile. The direction of the movement (rightward or leftward) was determined by the experiment.

4.5. Plasma characterization

The averaged Co density obtained in the plasma plume was $(2.5 \pm 0.3) \times 10^{16}$ cm^{-3}, where the error corresponds to the standard deviation. Results of the temperature in the plasma center are summarized in Fig. 8. Even though a linear growth of T_m with the laser pulse energy was observed (Fig. 8a), saturation is expected to be reached for a higher irradiance due to shielding effect. The evolution of T_m in the time interval considered is shown in Fig. 8b. An increase of the laser energy originated a growth of the temperature in the plasma center, and a raise in the line intensity, but the gradient of temperature was not affected. On the other hand, for each energy as the plasma cooled down with time, a drop of the line intensity was observed while the temperature gradient became less steep.

The employed experimental approach allows to obtain the line profiles of spectral emission intensities integrated along the line of sight. The model also makes it possible to carry on a spatially-resolved characterization of the plasma without need of any deconvolution procedure. This means to obtain the local values (in x-direction) of the main plasma parameters (the temperature and the number densities of electrons, atoms, and ions) within an

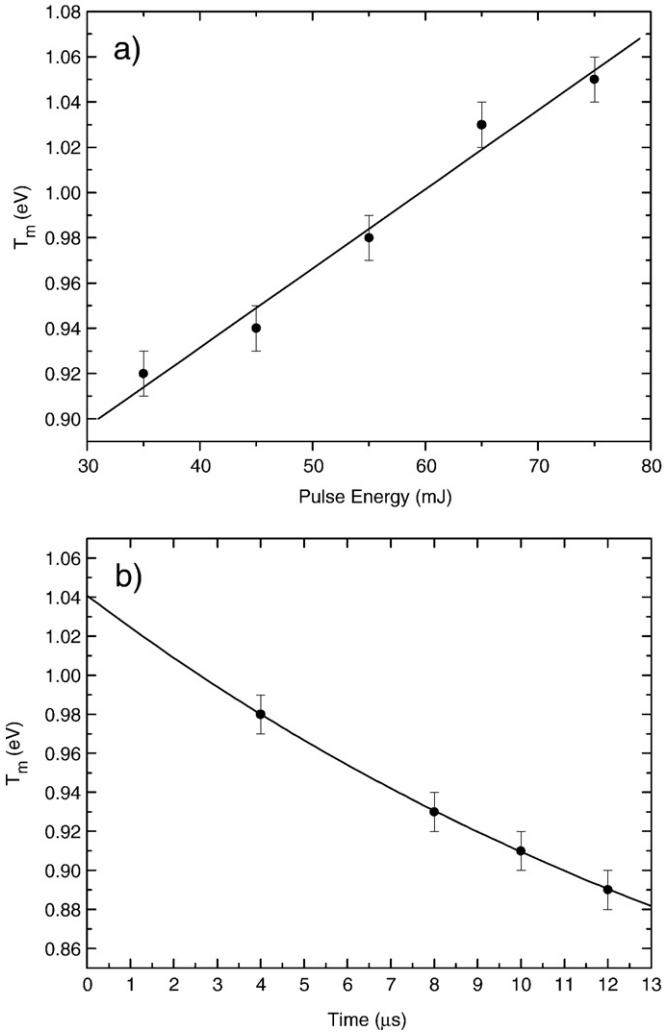

Fig. 8. a) Behavior of the maximum temperature at the plasma center with the pulse energy. b) Temporal evolution of the maximum temperature at the plasma center.

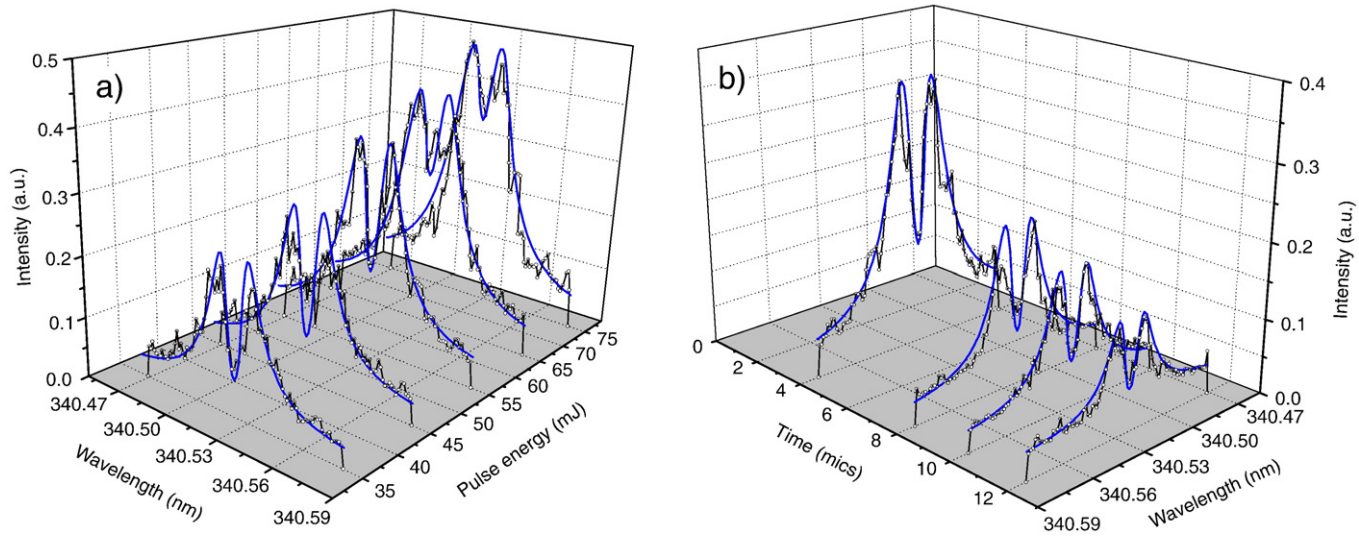

Fig. 7. Experimental (--o--) and computed (----) profiles of the line 340.51 Co I a) for different laser energies, and b) for different delay times.

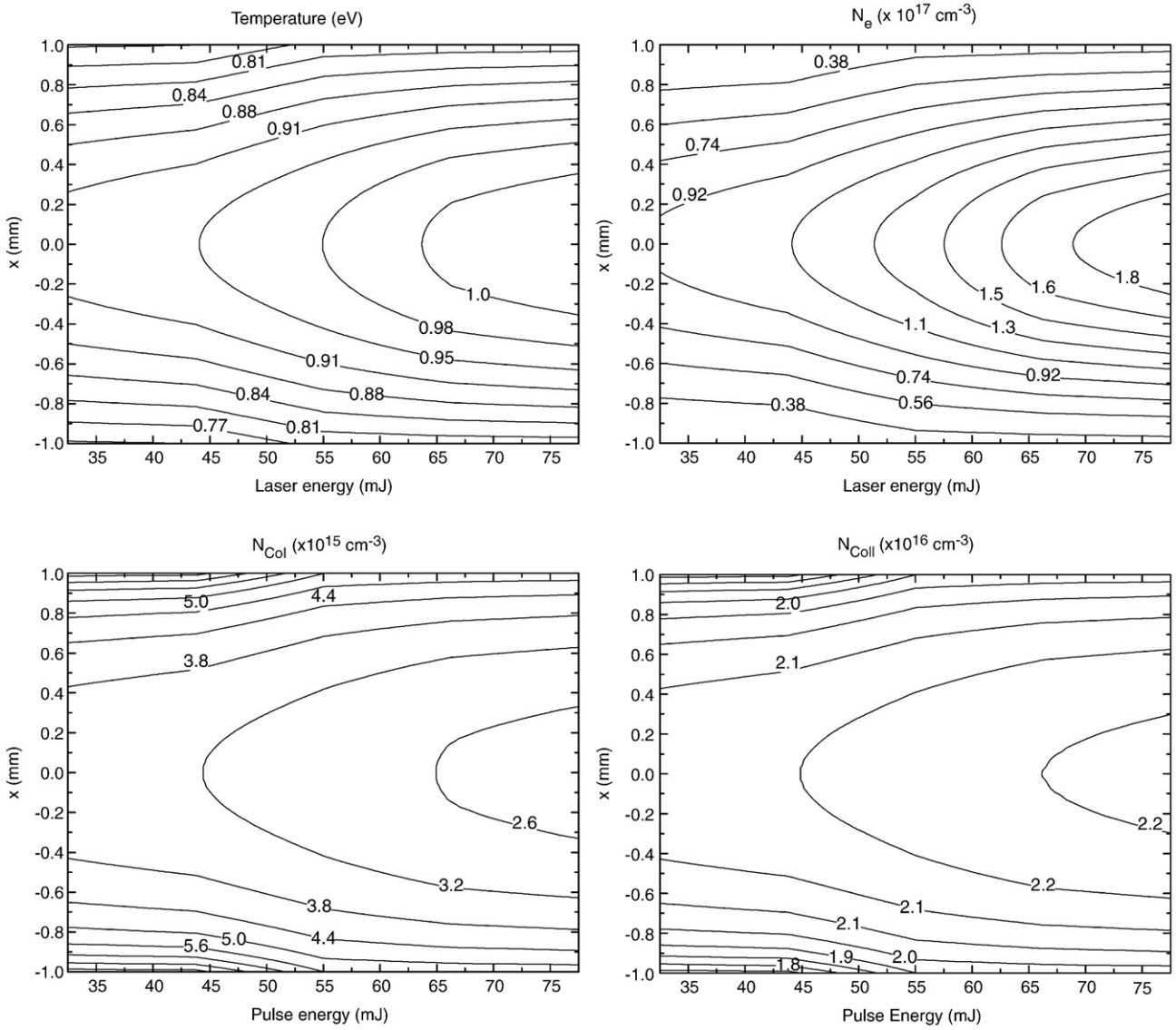

Fig. 9. Spatially-resolved results showing the effect of the laser irradiance distributions of temperature, electron, atom, and ion densities.

optically thick inhomogeneous LIP slice, normal to the laser beam, from the measured line profiles. In fact, starting from the distribution of temperature, given by T_m and b parameters of Eq. (11), and using the Saha–Boltzmann equations, the distributions of electron density and atom/ion densities can be easily calculated assuming the existence of LTE. Some results are exposed in Figs. 9 and 10. In Fig. 9, the effect of laser irradiance on the distributions of temperature, electron density, and atom and ion densities found in the LIP are shown. In Fig. 10, the time evolution of the temperature distribution, together with the electron, atom and ion densities distributions for a slice of plasma perpendicular to the direction of the laser beam are shown. We can appreciate that the temperature drops as the plasma experiences a cooling process. The electron density has a similar behavior following the temperature gradient. In general, the maximum of the distribution is obtained in a central region of the plasma, with a decrease toward the edges. In contrast, the maxima of the density of Co I atoms are near the plasma boundary, and there is a pronounced minimum at the center of the profile related to a high degree of ionization of the plasma. Besides, all distributions present a lower gradient at late times (>6 μs). Nevertheless, these are only preliminary results and a further rigorous study should be accomplished.

5. Conclusions

The aim of the present work is the investigation of laser-induced plasma characterization through the study of experimentally measured line profiles of selected spectral transitions.

Laser-induced plasmas generated on a metallic alloy have been characterized for different pulse energies (in the range 35–75 mJ) and delay times (in the range 4–12 μs), by a method based on computing the theoretical emission profiles of spectral lines and matching them to the experimental ones in the frame of a simple plasma model. The model describes an optically thick inhomogeneous plasma in LTE. The input parameters are the plasma length, the plasma temperature, which was simulated by a second-order parabola with its maximum in the plasma center, and the Co total density. These parameters allowed the calculation of the emission line intensities. They were estimated from measurements and adjusted in order to reproduce the measured profile of the analytical line Co I 340.51 nm. The outputs are spatial and temporal distributions of species in the plasma plume (atoms, ions and electrons). The applicability of the model was evaluated analyzing the influence of laser pulse energy and time evolution of the plasma.

In this approach, results showed that an increase of the pulse energy involved a growth of the maximum temperature in the plasma

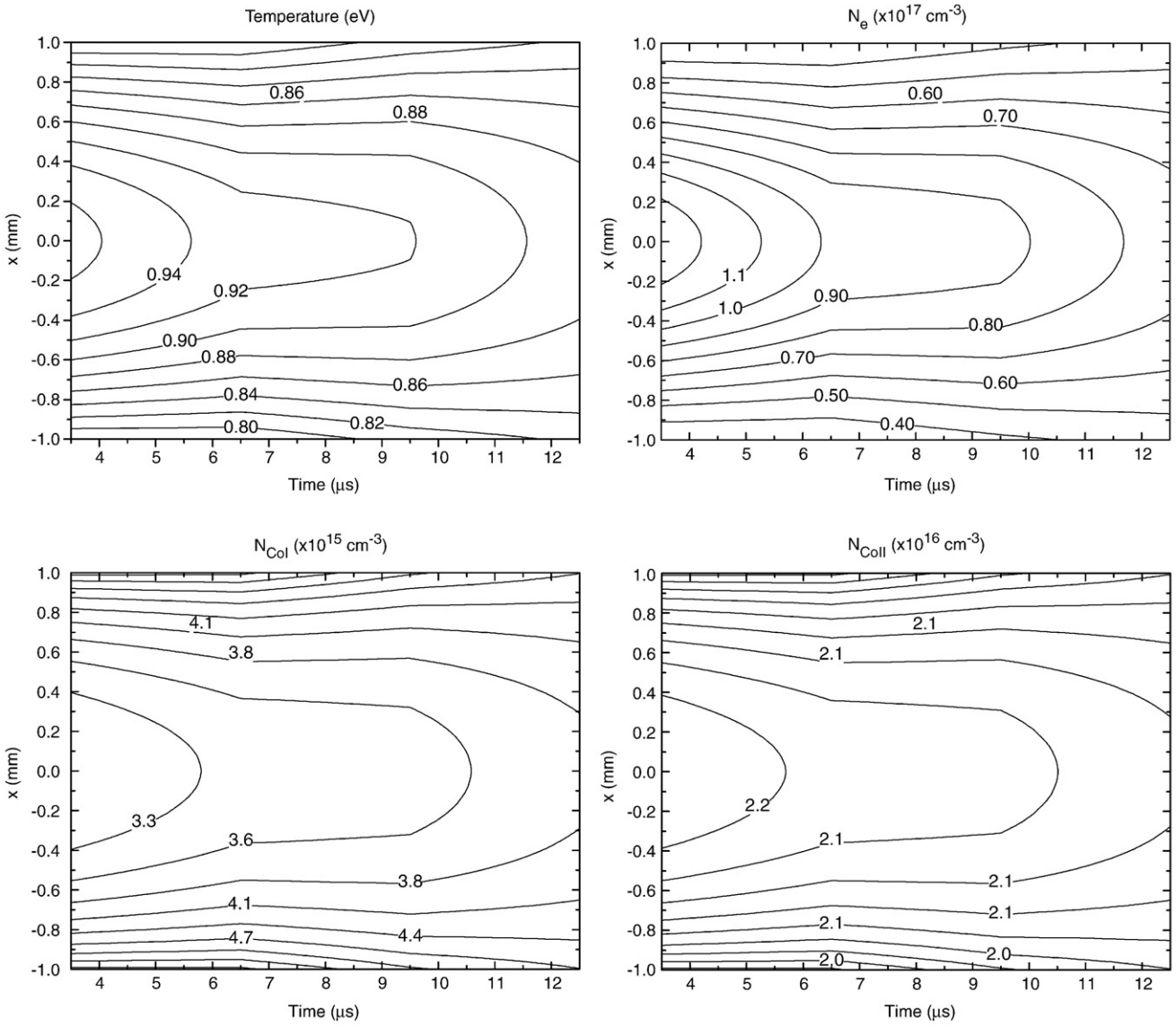

Fig. 10. Spatially-resolved results showing the temporal evolution of distributions of temperature, electron, atom, and ion densities.

core, and a consistent raise in the line intensity. Nevertheless, the plasma homogeneity, given by the gradient of temperature, was not affected by the laser irradiance on the sample surface. On the other hand, for each energy as the time progresses and the plasma cooled down, a drop of the line intensity was observed while it became more homogeneous. Thus, we can deduce that the presence of a central dip in the line profile is a sure sign that the line is being strongly absorbed in a non-uniform plasma. Nevertheless, we cannot conclude that the depth of the dip indicates a plasma more or less homogeneous. It is worth mentioning that, as shown in the work of reference [32], boundary effects, i.e.: shock wave front, are significant in a plasma into ambient gas. Nevertheless, it was considered a good approach to neglect them and use a parabolic temperature distribution. We were based on the experimental observation that a strong self-reversal was observed for the Co I 340.51 nm line due to absorption in the cold peripheral plasma layers.

Moreover, calculus of spatially-resolved distribution of parameters inside the plasma along the direction of observation can be easily performed, without the use of a deconvolution procedure. Some preliminary results were obtained suggesting a great potential in spectroscopic applications.

References

[1] E. Tognoni, V. Palleschi, M. Corsi, G. Cristoforetti, Quantitative microanalysis by laser-induced breakdown spectroscopy: a review of the experimental approaches, Spectrochim. Acta Part B 57 (2002) 1115–1130.
[2] C. Aragón, J.A. Aguilera, Characterization of laser induced plasmas by optical emission spectroscopy: a review of experiments and methods, Spectrochim. Acta Part B 69 (2008) 893–916.
[3] Aragón, J. Bengoechea, J.A. Aguilera, Asymmetric Stark broadening of the Fe I 538.34 nm emission line in a laser induced plasma, Spectrochim. Acta Part B 60 (2005) 897–904.
[4] J. Bengoechea, J.A. Aguilera, C. Aragón, Application of laser-induced plasma spectroscopy to the measurement of Stark broadening parameters, Spectrochim. Acta Part B 61 (2006) 69–80.
[5] C. Colón, A. Alonso-Medina, Application of a laser produced plasma: experimental Stark widths of single ionized lead lines, Spectrochim. Acta Part B 61 (2006) 856–863.
[6] F. Bredice, F.O. Borges, H. Sobral, M. Villagran-Muniz, H.O. Di Rocco, G. Cristoforetti, S. Legnaioli, V. Palleschi, A. Salvetti, E. Tognoni, Measurement of Stark broadening of Mn I and Mn II spectral lines in plasmas used for Laser-Induced Breakdown Spectroscopy, Spectrochim. Acta Part B 62 (2007) 1237–1245.
[7] F. Bredice, F.O. Borges, H. Sobral, M. Villagran-Muniz, H.O. Di Rocco, G. Cristoforetti, S. Legnaioli, V. Palleschi, L. Pardini, A. Salvetti, E. Tognoni, Evaluation of self-absorption of manganese emission lines in Laser Induced Breakdown Spectroscopy measurements, Spectrochim. Acta Part B 61 (2006) 1294–1303.
[8] H.O. Di Rocco, D.I. Iriarte, J.A. Pomarico, Lifetimes and transition probabilities of Xe II: experimental measurements and theoretical calculations, Eur. Phys. J. D 10 (2000) 19–26.

[9] M. Sabsabi, P. Cielo, Quantitative analysis of aluminum alloys by laser-induced breakdown spectroscopy and plasma characterization, Appl. Spectrosc. 49 (1995) 499–507.
[10] J.M. Gomba, C. D'Angelo, D. Bertuccelli, G. Bertuccelli, Spectroscopic characterization of laser induced breakdown in aluminum–lithium alloy samples for quantitative determination of traces, Spectrochim. Acta Part B 56 (2001) 695–705.
[11] J.A. Aguilera, C. Aragón, Characterization of laser-induced plasmas by emission spectroscopy with curve-of-growth measurements. Part I: temporal evolution of plasma parameters and self-absorption, Spectrochim. Acta Part B 63 (2008) 784–792.
[12] J.A. Aguilera, C. Aragón, Characterization of laser-induced plasmas by emission spectroscopy with curve-of-growth measurements. Part II: effect of the focusing distance and the pulse energy, Spectrochim. Acta Part B 63 (2008) 793–799.
[13] C. Aragón, J. Bengoechea, J.A. Aguilera, Influence of the optical depth on spectral line emission from laser-induced plasmas, Spectrochim. Acta Part B 56 (2001) 619–628.
[14] C. Aragón, F. Peñalba, J.A. Aguilera, Curves of growth of neutral atom and ion lines emitted by a laser induced plasma, Spectrochim. Acta Part B 60 (2005) 879–887.
[15] J.A. Aguilera, J. Bengoechea, C. Aragón, Spatial characterization of laser induced plasmas obtained in air and argon with different laser focusing distances, Spectrochim. Acta Part B 59 (2004) 461–469.
[16] J.A. Aguilera, C. Aragón, Characterization of a laser-induced plasma by spatially resolved spectroscopy of neutral atom and ion emissions. Comparison of local and spatially integrated measurements, Spectrochim. Acta Part B 59 (2004) 1861–1876.
[17] M. Ferretti, G. Cristoforetti, S. Legnaioli, V. Palleschi, A. Salvetti, E. Tognoni, E. Console, P. Palaia, In situ study of the Porticello Bronzes by portable X-ray fluorescence and laser-induced breakdown spectroscopy, Spectrochim. Acta Part B 62 (2007) 1512–1518.
[18] A. De Giacomo, M. Dell'Aglio, O. De Pascale, S. Longo, M. Capitelli, Laser induced breakdown spectroscopy on meteorites, Spectrochim. Acta Part B 62 (2007) 1606–1611.
[19] A. De Giacomo, M. Dell'Aglio, O. De Pascale, R. Gaudiuso, A. Santagata, R. Teghil, Laser Induced Breakdown Spectroscopy methodology for the analysis of copper-based-alloys used in ancient artworks, Spectrochim. Acta Part B 63 (2008) 585–590.
[20] J.M. Anzano, M.A. Villoria, A. Ruíz-Medina, R.J. Lasheras, Laser-induced breakdown spectroscopy for quantitative spectrochemical analysis of geological materials: effects of the matrix and simultaneous determination, Anal. Chim. Acta 575 (2006) 230–235.
[21] B. Sallé, J.-L. Lacour, P. Mauchien, P. Fichet, S. Maurice, G. Manhès, Comparative study of different methodologies for quantitative rock analysis by Laser-Induced Breakdown Spectroscopy in a simulated Martian atmosphere, Spectrochim. Acta Part B 61 (2006) 301–313.
[22] S. Laville, M. Sabsabi, F.R. Doucet, Multi-elemental analysis of solidified mineral melt samples by Laser-Induced Breakdown Spectroscopy coupled with a linear multivariate calibration, Spectrochim. Acta Part B 62 (2007) 1557–1566.
[23] D. Bulajic, M. Corsi, G. Cristoforetti, S. Legnaioli, V. Palleschi, A. Salvetti, E. Tognoni, A procedure for correcting self-absorption in calibration free-laser induced breakdown spectroscopy, Spectrochim. Acta Part B 57 (2002) 339–353.
[24] P. Yaroshchyk, D. Body, R. Morrison, B. Chadwick, A semi-quantitative standardless analysis method for laser-induced breakdown spectroscopy, Spectrochim. Acta Part B 61 (2006) 200–209.
[25] J. Hermann, C. Boulmer-Leborgne, D. Hong, Diagnostic of the early phase of an ultraviolet laser induced plasma by spectral line analysis considering self-absorption, J. Appl. Phys. 83 (2) (1998) 691–696.
[26] J.A. Aguilera, J. Bengoechea, C. Aragón, Curves of growth of spectral lines emitted by a laser-induced plasma: influence of the temporal evolution and spatial inhomogeneity of the plasma, Spectrochim. Acta Part B 58 (2003) 221–237.
[27] J.A. Aguilera, C. Aragón, J. Bengoechea, Spatial characterization of laser-induced plasmas by deconvolution of spatially resolved spectra, Appl. Opt. 42 (2003) 5938–5946.
[28] J.A Aguilera, C. Aragón, Characterization of a laser-induced plasma by spatially resolved spectroscopy of neutral atom and ion emissions: comparison of local and spatially integrated measurements, Spectrochim. Acta Part B 59 (2004) 1861–1876.
[29] J.A. Aguilera, J. Bengoechea, C. Aragón, Spatial characterization of laser induced plasmas obtained in air and argon with different laser focusing distances, Spectrochim. Acta Part B 59 (2004) 461–469.
[30] I.B. Gornushkin, C.L. Stevenson, B.W. Smith, N. Omenetto, J.D. Winefordner, Modeling an inhomogeneous optically thick laser induced plasma: a simplified theoretical approach, Spectrochim. Acta Part B 56 (2001) 1769–1785.
[31] H. Zwicker, Evaluation of plasma parameters in optically thick plasmas, in: W. Loghte-Holtgreven (Ed.), Plasma Diagnostics, Amsterdam, 1968.
[32] A.Ya. Kazakov, B. Gornushkin, N. Omenetto, B.W. Smith, J.D. Winefordner, Radiation dynamics of post-breakdown laser induced plasma expanding into ambient gas, Appl. Opt. 45 (2006) 2810–2820.
[33] I.B. Gornushkin, N. Omenetto, B.W. Smith, J.D. Winefordner, Determination of the maximum temperature at the center of an optically thick laser-induced plasma using self-reversed spectral lines, Spectrochim. Acta Part B 59 (2004) 401–418.
[34] C.A. D'Angelo, D.M. Díaz Pace, G. Bertuccelli, D. Bertuccelli, Laser induced breakdown spectroscopy on metallic alloys: solving inhomogeneous optically thick plasmas, Spectrochim. Acta Part B 63 (2008) 367–374.
[35] L.J. Radziemsky, D.A. Cremers, Laser-Induced Plasmas and Applications, Marcel Dekker Inc, New York, 1989.
[36] I.I. Sobelman, Atomic Spectra and Radiative Transitions, Springer, Berlin, 1979.
[37] N. Konjevic, J.R. Roberts, A critical review of the Stark widths and shifts of spectral lines from non-hydrogenic atoms, J. Phys. Chem. Ref. Data 5 (1976) 209–257.